Ultramicroscopy 202 (2019) 156–162

Contents lists available at ScienceDirect

Ultramicroscopy

journal homepage: www.elsevier.com/locate/ultramic

Direct observation of magnetic contrast obtained by photoemission electron microscopy with deep ultra-violet laser excitation

Zhao Y.C.[a,b], Lyu H.C.[a,c], Yang G.[a,c], Dong B.W.[a,c], Qi J.[c], Zhang J.Y.[c], Zhu Z.Z.[a], Sun Y.[a], Yu G.H.[c], Jiang Y.[c], Wei H.X.[a], Wang J.[a], Lu J.[a], Wang Z.H.[a], Cai J.W.[a], Shen B.G.[a], Zhan W.S.[a], Yang F.[d], Zhang S.J.[d], Wang S.G.[a,c,*]

[a] State Key Laboratory of Magnetism, Institute of Physics, Chinese Academy of Sciences, Beijing 100190, China
[b] School of Physical Sciences, University of Chinese Academy of Sciences, Beijing 100049, China
[c] Beijing Advanced Innovation Center for Materials Genome Engineering, School of Materials Science and Engineering, University of Science and Technology Beijing, Beijing 100083, China
[d] Key Lab of Functional Crystals and Laser Technology, Technical Institute of Physics and Chemistry, Chinese Academy of Sciences, Beijing 100190, China

ARTICLE INFO

Keywords:
Photoemission electron microscopy
Magnetic domain imaging
Deep ultraviolet laser

ABSTRACT

Magnetic circular dichroism (MCD) and magnetic linear dichroism (MLD) have been investigated in a photoemission electron microscopy (PEEM) system excited by a deep ultra-violet (DUV) laser (with $\lambda = 177.3$ nm and $h\upsilon = 7.0$ eV) for the first time. High resolution PEEM magnetic images (down to 43.2 nm) were directly obtained on a (001)-oriented magnetic FePt film surface with a circularly-polarized light under normal incidence. Furthermore, a stepped Cr seeding layer was applied to induce the formation of large-area epitaxial FePt films with (001) and (111) two orientations, where MLD with large asymmetry was observed in the transition area of two phases. It demonstrates that DUV laser can be a powerful source for high resolution magnetic imaging in the laboratory in absence of synchrotron facilities.

1. Introduction

As a newly evolving field, spintronics has become an important research area in information technology, such as data storage and logical devices [1–3]. Ferromagnetic materials with characteristic spin-polarization play a fundamental role in nano-scaled spintronic structures. Furthermore, the study with a focus on magnetic properties of multilayered films has attracted more and more interests, especially the magnetic domain structures dominated by surface and interface. This creates an urgent demand of characterization techniques for magnetic domains with high spatial resolution on a microscopic scale [4]. Among methods for magnetic domain imaging, photoemission electron microscopy (PEEM) is sensitive to the spectroscopic information directly from the magnetic films and surfaces through photoemission process with variable excitation sources [5,6]. A typical choice to obtain the magnetic contrast is x-ray PEEM (X-PEEM), a combination of PEEM and synchrotron radiation light source [7–9]. By using monochromatic x-rays with circular or linear polarizations, the domain images based on magnetic circular dichroism (MCD) and magnetic linear dichroism (MLD) can be obtained by the secondary electron intensity distribution at the sample surface [10–15]. Both the elemental and magnetic specificity make it a considerably powerful tool to investigate the magnetic domains. However, X-PEEM can only be equipped in synchrotron facilities, and the limited beam time together with confined space to accommodate both *in situ* molecular beam epitaxy (MBE) system and PEEM make it difficult to be widely applied. Therefore, it is extremely attractive to carry out research on the nano-scaled magnetic domains in the laboratory, where the high-quality thin films can be *in situ* grown and characterized simultaneously based on PEEM.

Recently, threshold PEEM system using light sources with photon energy close to the typical values of work function have been applied to investigate the magnetic contrast both in theoretical [16–18] and experimental studies. For example, a MLD asymmetry of 0.37% was observed by Marx et al. on a 100 nm Fe film using PEEM equipped with a mercury arc lamp with UV photon energy of 4.9 eV [19]. Furthermore, circularly polarized laser light with different wavelengths such as 635 nm [20–22], 405 nm [23], 325 nm [20–22] and 267 nm [24] were applied to perform MCD measurements, respectively. The pioneering work above provides a novel method to investigate surface magnetic domains by photoemission technique. For a typical excitation by laser

* Corresponding authors at: Beijing Advanced Innovation Center for Materials Genome Engineering, School of Materials Science and Engineering, University of Science and Technology Beijing, Beijing 100083, China.
E-mail address: sgwang@ustb.edu.cn (S.G. Wang).

https://doi.org/10.1016/j.ultramic.2019.04.009
Received 11 December 2018; Received in revised form 31 March 2019; Accepted 17 April 2019
Available online 18 April 2019
0304-3991/

sources in threshold PEEM system, a usual process to reduce the work function by depositing caesium was used [20–23]. Another direct way to overcome the work function is to use excitation sources with higher photon energy. Deep ultraviolet (DUV) laser light is a considerable choice to provide higher photon energy. Previous work by using 266 nm laser with photon energy of 4.66 eV was performed in aberration-corrected PEEM system [25]. However, a Cs deposition process is still necessary to obtain magnetic contrast of perpendicular FePt thin films although 4.66 eV is close to the work function of 3*d* magnetic metals (4.5 eV, 5.0 eV and 5.2 eV for Fe, Co and Ni, respectively [26]).

As a powerful source, the DUV laser (λ = 177.3 nm, $h\nu$ = 7.0 eV) has been proved to be a reliable and efficient choice for photoemission technique on surface investigation in PEEM system with high spatial resolution [27] and angle-resolved photoemission spectroscopy (ARPES) with an energy resolution better than 1 meV [28]. In this work, the 177.3 nm DUV laser with variable polarizations was applied as an excitation source in a PEEM system to carry out a detailed study on the magnetic contrast. The domain patterns with high resolution of 43.2 nm was observed directly based on both MCD and MLD for *in situ* epitaxially grown FePt films, demonstrating the feasibility of the DUV-PEEM as a solution for magnetic imaging with high spatial resolution.

2. Materials and methods

2.1. Sample fabrication

A set of $Fe_{50}Pt_{50}$ films with different structures of the buffer layer were prepared on polished MgO (001) single crystal substrates by using a molecular beam epitaxy (MBE) system with base vacuum better than 7.0×10^{-11} mbar. The MgO substrates were cleaned by acetone in an ultrasound bath prior to the deposition and annealed at 750 °C in the MBE chamber for 2 h after a 20-min degas process at 850 °C to form a clean surface which was further characterized *in situ* by reflection high-energy election diffraction for epitaxial growth. The thickness of FePt layer was 20 nm, where Fe and Pt were co-evaporated by electron beam heating with separated sources. Substrate temperatures for FePt deposition were set at 500 °C and room temperature (RT) to form the $L1_0$ phase and disorder phase, respectively. Cr growth was achieved by thermal evaporation source with the temperature of 1450 °C. The formation of a 5 nm thick Cr step was performed by setting an appropriate location of a gradient shutter between the effusion cell and the substrate to limit the evaporation beam area.

2.2. DUV-PEEM setup

The DUV-PEEM system with a base pressure better than 3×10^{-10} mbar is connected to the MBE chamber. Therefore, the sample can be immediately transferred to the DUV-PEEM analysis chamber when the deposition is accomplished. A 15-kV voltage is applied to the sample holder to accelerate the photoelectrons between the sample surface and the objective lens.

As shown in Fig. 1, three excitation sources are integrated in the FE-LEEM /PEEM P90 system (SPECS, GmbH). A 100 W Hg arc lamp produces UV photons with an energy of 4.9 eV. The angle of UV light incidence with respect to the microscope axis and the surface normal is about 75°. The deep ultraviolet from the diode-pumped laser (DUV-DPL) passes through the prism chamber and the objective lens, and it excites the sample at an angle of smaller than 5° in a nearly normal incidence geometry. For LEEM (Low Energy Electron Microscopy)/ LEED (Low Energy Electron Diffraction) observation, cold field emitter is applied as an electron source. Electron beam is generated by the electron gun and deflected over a 90° angle by magnetic array in prism chamber leading to a normal incidence to the sample surface. The best spatial resolution of PEEM and LEEM observation obtained in this system is 10 nm and 5 nm, respectively.

The 177.3 nm DUV laser light is produced by second-harmonic

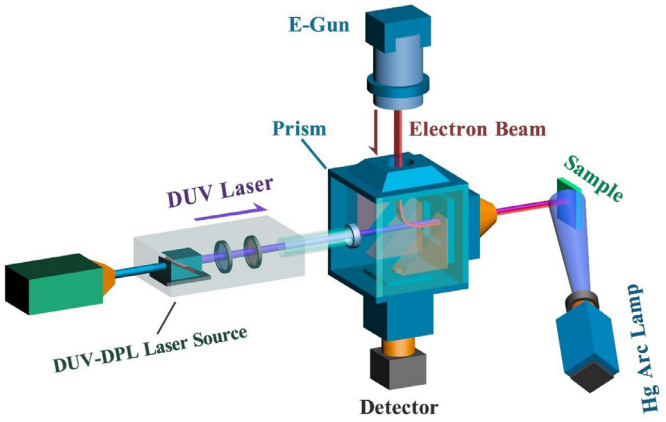

Fig. 1. A schematic layout of the DUV laser-based LEEM/PEEM system.

generation using a 355 nm UV laser and a prism-coupled technique (PCT) device with a $KBe_2BO_3F_2$ (KBBF) nonlinear optical crystal [29]. The photon energy of DUV is $h\nu$ = 7.0 eV, which is large enough to overcome usual work function of the metallic materials for photoemission process, even including some heavy metals such as Pt and Ir. Variable polarizations of DUV make it possible to carry out the MCD/ MLD PEEM experiments for magnetic domain imaging. As shown in Fig. 2, circular polarizations and helicity switching can be performed by introducing a rotatable quarter-wave plate in the laser path. Likewise, linear polarization of the DUV laser becomes controllable by changing the angle between the optical axis of a half-wave plate and the electric field vector ***E*** of the laser. A tube with CaF_2 windows on both ends and pumped by a turbo-molecular pump connects the DUV laser source and the PEEM system. After evacuation, the laser chamber and the tube are filled with high purity nitrogen to ensure a high efficiency of DUV transmission during the experiments. The laser pulses have a duration of 12 ps and repetition rate of 118.3 MHz, and the spot size is less than 1 mm in diameter. Due to the space charge effect [22,30] and an appropriate acquisition time, the output power is chosen at 320 μW to perform high resolution domain imaging.

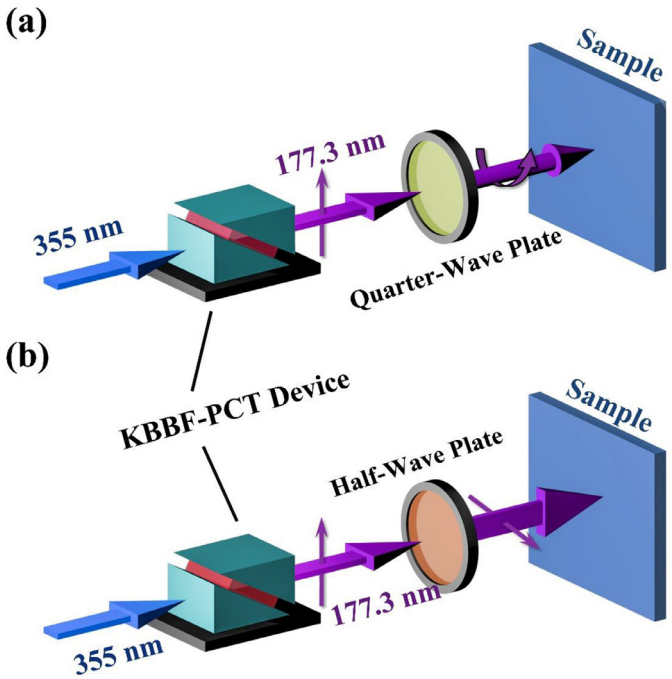

Fig. 2. Schematic drawings of the DUV laser optical system with circular (a) and linear (b) polarizations.

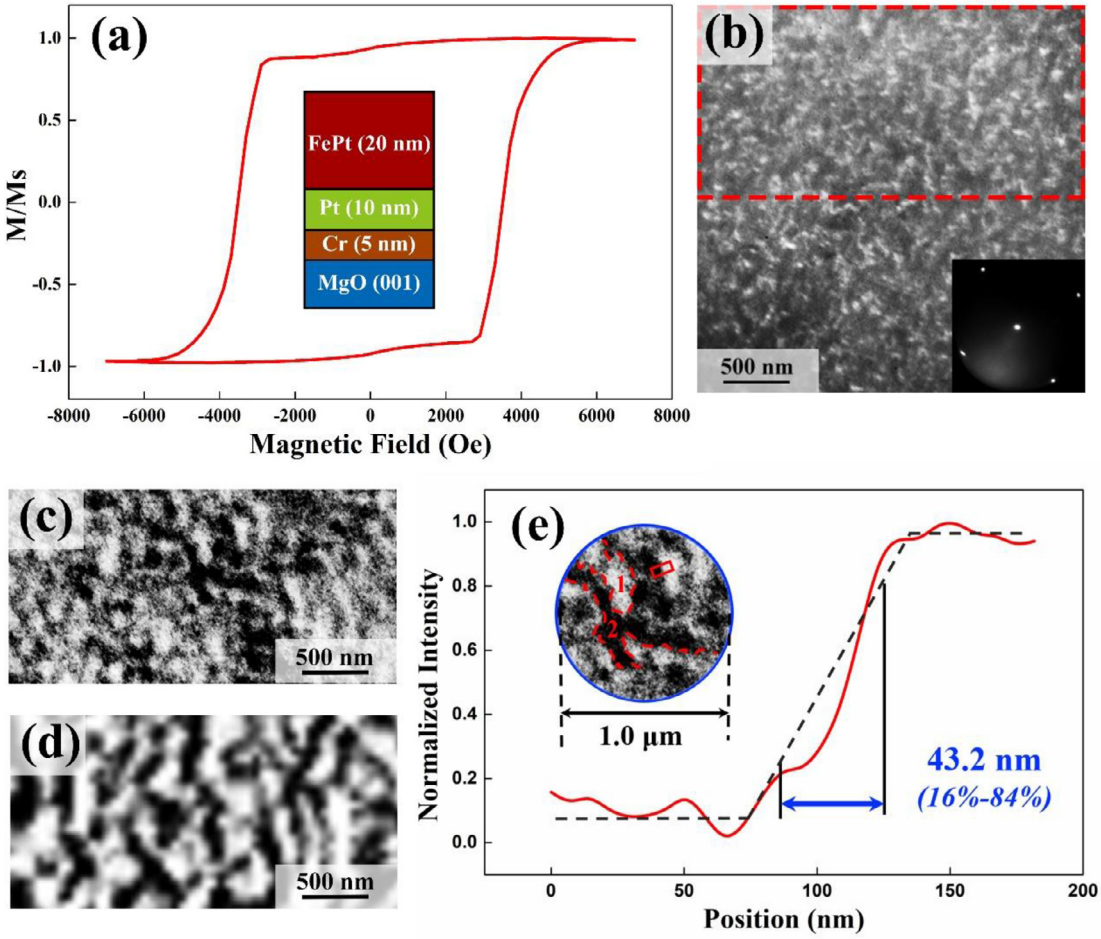

Fig. 3. (a) Schematic structure and out-of-plane hysteresis loop of MgO (001) sub. /Cr (5 nm)/Pt (10 nm)/FePt (20 nm grown at 500 °C) films. (b) LEEM image (E_p = 8.6 eV) and LEED (E_p = 16.3 eV) pattern (inset) of FePt film. (c) Magnetic domain (contrast enhanced) of the area marked by a red dashed rectangle in (b) taken with circularly polarized DUV laser. (d) Magnetic domain image of the FePt films with the same structure obtained by magnetic force microscopy. (e) Normalized line profile with the estimated spatial resolution from selected area marked in inset. (For interpretation of the references to color in this figure legend, the reader is referred to the web version of this article.)

3. Results and discussion

The 20 nm thick $Fe_{50}Pt_{50}$ film with $L1_0$ ordered structure was deposited at 500 °C. The sample structure was MgO (001) /Cr (5 nm)/Pt (10 nm)/FePt (20 nm). A Cr seed layer was applied to induce the epitaxial growth of Pt buffer layer. The clean Pt (001)-oriented surface in favor of the FePt ordered phase formation was achieved after 30-min annealing at 600 °C for minimization of the lattice strain. Fig. 3(a) shows a schematic drawing of the $L1_0$ FePt sample structure and out-of-plane hysteresis loop obtained using the vibrating sample magnetometer (VSM). The coercivity was about 3500 Oe, indicating an ordered structure of FePt layer with perpendicular magnetic anisotropy (PMA). More details about the growth and magnetic properties can be found in Ref. [31,32].

Topographic observation was performed in LEEM mode using PEEM/LEEM system. The LEEM image (primary energy of the incident electrons, E_p = 8.6 eV) shown in Fig. 3(b) indicates a surface with island-like morphology, in good agreement with previous studies of $L1_0$ FePt film by atomic force microscopy (AFM) [33]. A (001)-oriented epitaxial relationship with a clean surface was confirmed by the sharp LEED pattern (E_p = 16.3 eV) as shown in inset of Fig. 3(b). By introducing the 177.3 nm DUV laser, photoelectrons can be excited without surface work function reduction because the photon energy ($h\nu$ = 7.0 eV) is much larger than the work function of general magnetic thin films (such as 5.0 eV). With normal incidence of circularly-polarized laser, the MCD contrast in photoemission from perpendicularly magnetized surface can be detected. A quarter-wave plate was placed with its axis at ± 45° from the linear polarization vector of the DUV laser to switch the helicity of circular polarization. For MCD-PEEM measurements, images with left (frame $_L$) and right (frame $_R$) circularly polarized DUV laser light were taken separately. 10 frames were collected (the integration time of each frame was 1500 ms) for the averaged image to obtain a sufficient signal-to-noise ratio. The MCD image was obtained by dividing the two normalized frames with opposite helicity on a pixel-by-pixel base so that the work function contrast, topographical contrast or other non-magnetic surface information can be suppressed [4]. Fig. 3(c) shows the measured magnetic domain image (contrast enhanced) of the selected area marked by a red dashed rectangle in Fig. 3(b) with the circularly polarized DUV laser light excitation. It is a typical labyrinth pattern of domain structure of $L1_0$ FePt film [33], and the similar image was further characterized by magnetic force microscopy (MFM) shown in Fig. 3(d). By comparison with the LEEM image, the magnetic domain contrast can be clearly distinguished from the surface topography. The spatial resolution can be estimated by the lateral distance between 16% and 84% of the maximum emission intensity. As shown in Fig. 3(e), the estimated resolution is obtained from the normalized intensity curve corresponding to a line profile of the selected area on the MCD image marked by the red rectangle in inset. The calculated value was approximately 43.2 nm, which is on same level as the spatial resolution of X-PEEM typically in the

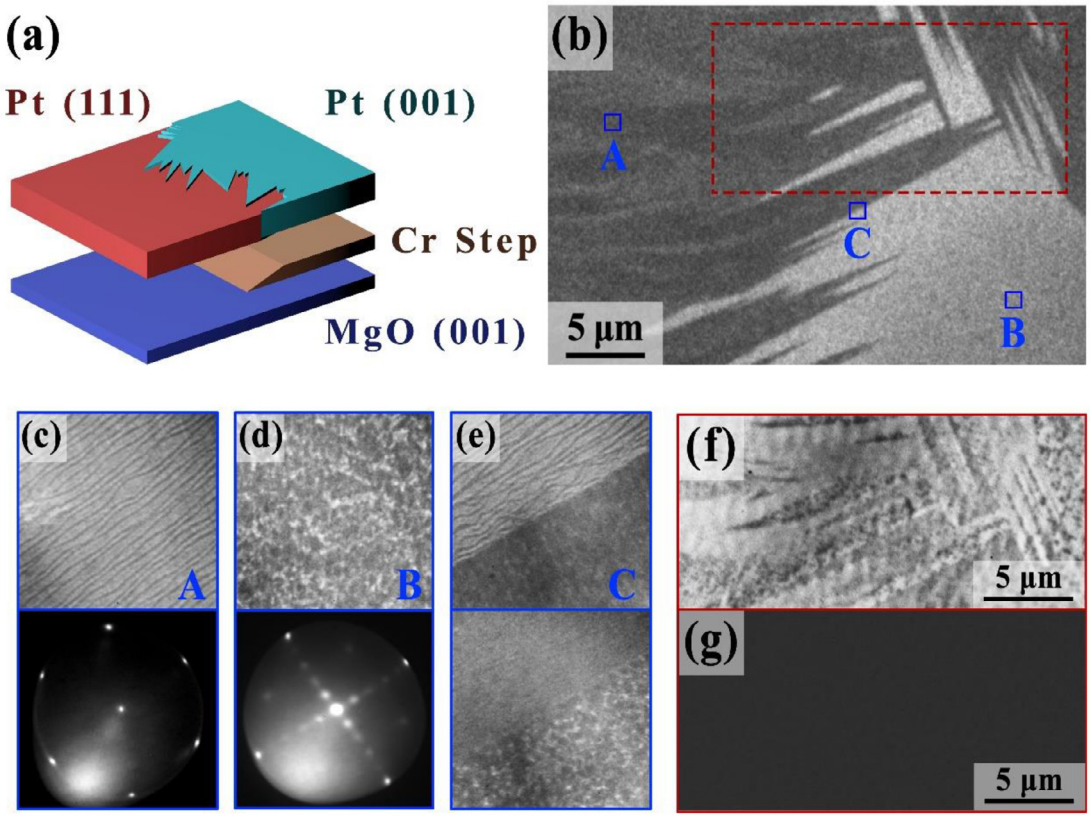

Fig. 4. (a) Schematic drawing of a Pt buffer layer with Cr step. (b) UV PEEM image of Pt buffer layer consisting of two orientations. LEEM and LEED patterns of the selected areas marked by blue rectangles in (b): (c) dark area A, (d) light area B and (e) boundary area C. (f) DUV PEEM image of the selected area marked by a red dashed rectangle in (b). (g) Linear dichroism image of the same area as (f). (For interpretation of the references to color in this figure legend, the reader is referred to the web version of this article.)

20–100 nm range for magnetic imaging [4,34–36]. The averaged MCD asymmetry,

$$A_{MCD} = \frac{(I_R/I_L)_1 - (I_R/I_L)_2}{(I_R/I_L)_1 + (I_R/I_L)_2} \quad (1)$$

between the light (1) and dark (2) areas in the ratio image shown in Fig. 3(e) was 2.2%, where I_R (I_L) is the emission intensity of frame $_L$ (frame $_R$). It was lower than the value in previous study using UV laser source with surface work function tuning [20]. For the higher DUV photon energy of 7.0 eV used here, the total magnetic dichroic signal is an average over all involved electronic states (around 2 eV below Fermi level for FePt), which may lead to a lower asymmetry. On the other hand, the DUV may also excite additional spin-orbit hot spots, which can increase the asymmetry. The final asymmetry is determined by above two effects [17,18,37].

Furthermore, orientated growth of FePt film was determined by the crystal structure of Pt buffer layer according to a parallel alignment of their epitaxial orientations. For Pt growth, (111)-oriented structure was formed directly onto the MgO (001) surface at room temperature due to interfacial energy minimum [38,39]. However, an epitaxial Pt (001) structure can be obtained after introducing a Cr seed layer on the MgO surface. Based on this, epitaxial FePt films with different structures can be achieved by this buffer layer process.

For 10 nm Pt buffer without Cr seed layer, (111)-orientated structure was formed, inducing a homogeneous crystal structure of 20 nm FePt layer. VSM results show that the magnetization of the (111)-oriented FePt film with in-plane magnetic anisotropy has a noticeable decrease (approximately 82%) compared with that of the ordered structure, and no MCD contrast can be observed on this sample. Moreover, for the two samples mentioned above, no clear MLD contrast was observed.

According to the above discussion about Pt growth on MgO (001) substrate, a buffer layer consisting of both (001) and (111) orientations was designed by introducing a Cr step across MgO surface. Fig. 4(a) shows a schematic drawing for the sample structure, and the Cr evaporation was controlled by a gradient shutter during the deposition to cover only half of the sample surface, forming a 5 nm Cr step in height. With this process, the two differently oriented structures of Pt (001) and (111) coexist, where each orientation covers half of the sample surface. As shown in Fig. 4(b), a UV PEEM image demonstrated the formation of a Pt surface with two oriented directions. Due to the difference in work function, 5.84 eV for Pt (001) surface and 5.93 for Pt (111) surface (experimental results through field-emission measurements in Ref. [40]), work function contrast could be observed between the dark and light areas, indicating the clear boundaries of the two oriented structures. Three areas, corresponding to dark area (A), light area (B) and boundary area (C) marked with blue rectangles on Fig. 4(b), were selected for LEEM and micro LEED observations. Fig. 4(c) presents the LEED pattern and the LEEM image of the area (A) with incident electrons of 26.8 eV and 11.2 eV, respectively. The well-spaced morphology with atomic steps can be observed from the LEEM image, and a typical (111)-oriented LEED pattern composed of sharp spots indicates an (111) orientation of the Pt surface in the selected area. The (001)-oriented structure in area (B) was confirmed by the LEED pattern (E_p = 16.3 eV) of 5 × 1 reconstruction shown in Fig. 4(d). An island-like Pt (001) surface topography shown in the LEEM image (Fig. 4(d), E_p = 3.8 eV) suggests a completely different morphological feature from that of Pt (111) surface. The boundary between these two phases can be clearly recognized by LEEM images shown in Fig. 4(e). Accordingly, both work function contrast and topographic difference indicate the effect of Cr step to the coexistence state of Pt (001) and Pt (111) structures. Fig. 4(f) shows a PEEM image obtained by introducing the

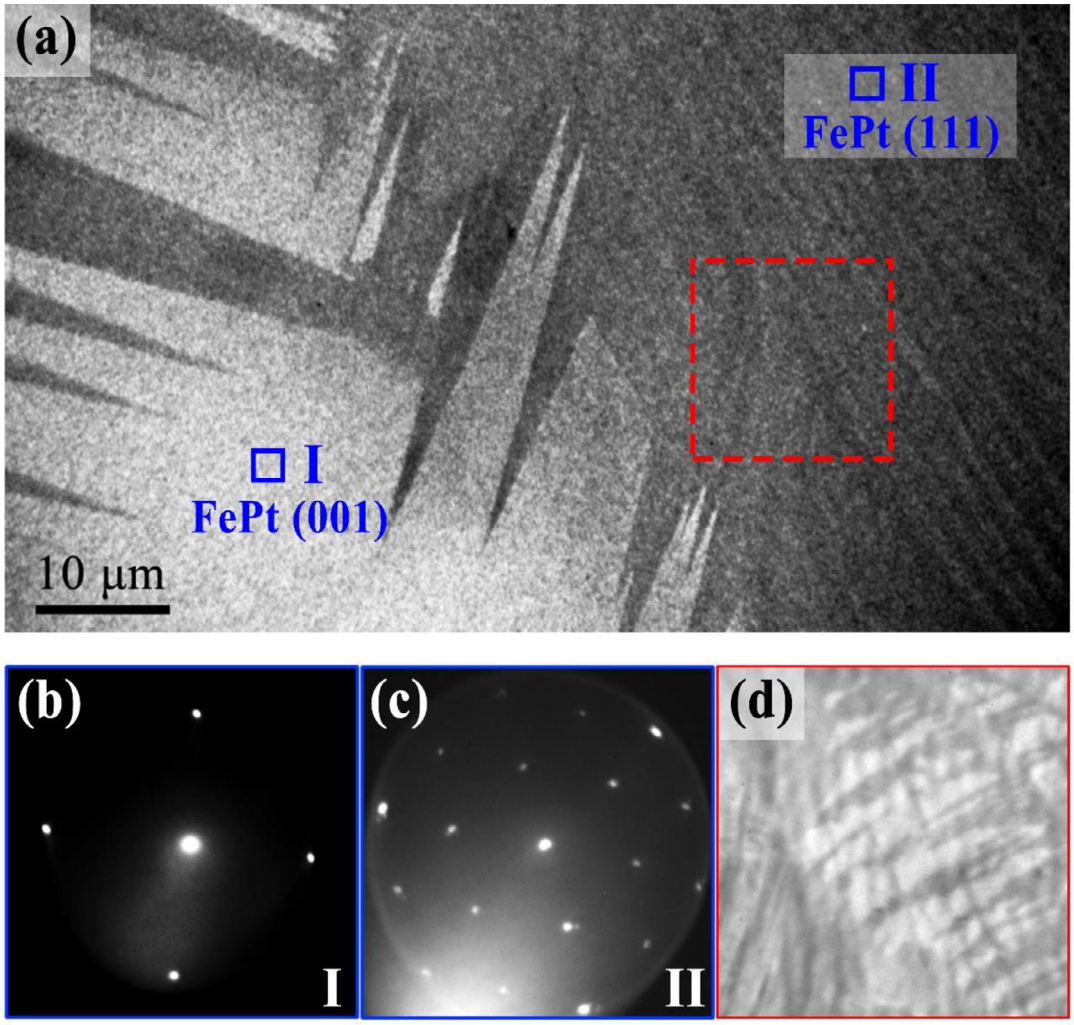

Fig. 5. (a) UV PEEM image of FePt film deposited on Pt buffer and Cr seed layer with two orientations. LEED patterns of selected areas marked by blue rectangles in (a): (b) light area I and (c) dark area II. (d) DUV-PEEM image of the selected area marked by a red dashed rectangle in (a) taken with linearly polarized laser. (For interpretation of the references to color in this figure legend, the reader is referred to the web version of this article.)

DUV laser of a selected area marked by the red dashed rectangle in Fig. 4(b). Compared with the results by UV light excitation, more surface details can be observed. Fig. 4(g) shows the results with linear dichroism obtained by two images taken with polarizations of light that differ by 90°, and no clear contrast can be seen. A similar result was obtained in the circular dichroism measurement, indicating that non-magnetic contrast caused by other mechanisms such as work function contrast and topographical contrast is significantly reduced in the final ratio image.

Based on this buffer layer with special structures mentioned above, 20 nm FePt film with (001) and (111) crystalline orientations was epitaxially grown. UV PEEM image shown in Fig. 5(a) indicates clear boundaries between the dark and light areas after FePt deposition at 500 °C. The FePt structure can be confirmed by micro-LEED observation on the selected areas marked by blue rectangles in Fig. 5(a). Fig. 5(b) shows the micro-LEED pattern at 16.3 eV on area I, indicating a (001)-oriented FePt film in the light area. Furthermore, a LEED pattern of the (111)-oriented surface [shown in Fig. 5(c), E_p = 31.9 eV] can be observed in dark area II. The LEED patterns indicate the epitaxial relation between the Pt buffer and the FePt layer. Similar to the results of UV PEEM image of Pt buffer layer, a work function difference between the two different orientations can be found. The dark area corresponds to the (111) orientation, which results from a higher surface work function. A dark area marked by the red dashed rectangle with a size of 15 μm × 15 μm was selected near the boundary of two phases for DUV laser PEEM observation. Both circularly polarized and linearly polarized DUV laser light were applied to investigate magnetic dichroism. Fig. 5(d) shows the PEEM image of selected area taken with linearly polarized DUV. It clearly indicates that more surface fine structures can be observed with the higher photon energy.

For MCD measurement, the same method for FePt sample with a (001)-oriented structure was investigated. Fig. 6(a) and (b) show the DUV PEEM images taken with left and right-circularly polarized (LCP, RCP) light respectively. To eliminate non-magnetic contrast, the image with RCP light was divided by the one with LCP light. Finally, the magnetic domain images can be obtained as shown in Fig. 6(c). The domains observed on this area have a much larger size than those shown in Fig. 3(c). By applying Eq. (1), an averaged MCD asymmetry between the light (1) and dark areas (2) in the radio image shown in Fig. 6(c) is 2.5%.

Our DUV-PEEM observation shown in Fig. 3 indicates a negligible MLD contrast for FePt films with single crystal structure. The similar method was performed for MLD measurements of the (001) and (111)-oriented FePt films. Fig. 6(d) and (e) show the DUV-PEEM images taken with linearly polarized light from the same area in Fig. 6(a–c). The polarizations were shown by red arrows in both images. Compared with the MCD results shown in Fig. 6(a–b), a more obvious magnetic contrast with the same domain patterns can be directly observed from MLD

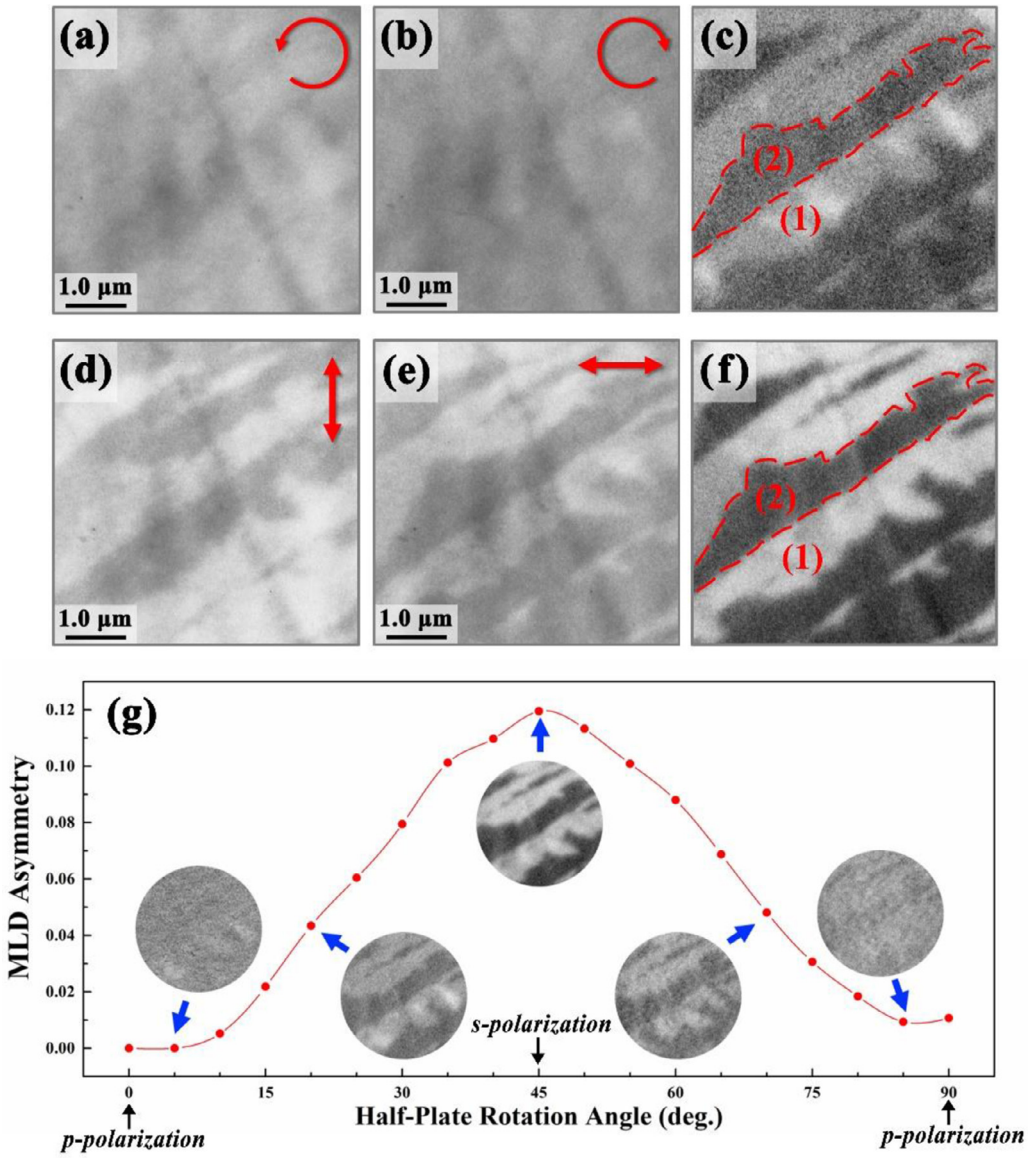

Fig. 6. DUV-PEEM images taken with (a) left-circularly polarized and (b) right-circularly polarized light. (c) MCD image of FePt film. (d)-(e): DUV-PEEM images taken with linearly-polarized laser (polarization shown by red arrow). (f) MLD imaged of FePt film. (g) Polarization dependent MLD asymmetry for the selected area (field of view in insets: 4 μm in diameter). (For interpretation of the references to color in this figure legend, the reader is referred to the web version of this article.)

measurements shown in Fig 6(d) without any further image processing, indicating that the magnetic information of this area is more selectively excited by linearly polarized DUV. By placing the axis of the half-wave plate at 45° from the electric field vector of the incident light, the direction of polarization will be changed by 90°. As shown in Fig. 6(e), magnetic contrast is reversed when the DUV polarization is rotated by 90°. Fig. 6(f) shows the MLD images obtained by a similar measurement as that for the MCD. With the improved signal-to-noise ratio due to a higher magnetic contrast, the MLD asymmetry:

$$A_{MLD} = \frac{(I_{\leftrightarrow}/I_{\updownarrow})_1 - (I_{\leftrightarrow}/I_{\updownarrow})_2}{(I_{\leftrightarrow}/I_{\updownarrow})_1 + (I_{\leftrightarrow}/I_{\updownarrow})_2} \quad (2)$$

between the light (1) and dark (2) areas in the radio image shown in Fig. 6(f) is 11.5%, where $I_{\leftrightarrow}$ and $I_{\updownarrow}$ is the intensity of PEEM images with corresponding polarizations, respectively. The MLD asymmetry is 4.6 times larger than that of MCD asymmetry. The best spatial resolution of the magnetic domains obtained by linearly polarized DUV laser was estimated as 47.1 nm which is similar to that of the MCD measurements in Fig. 3(d).

The polarization dependence of the MLD asymmetry was studied by varying the angel between the axis of the half-wave plate and the initial direction of laser polarization, in analogy to earlier x-ray [41] and laser [42] experiments of multiferroic $BiFeO_3$ system with a tunable polarization. As shown in Fig. 6(g), the measured asymmetry was increased from 0 to 11.5%, reaching the maximum at 45° corresponding to a 90° deflection of polarization. With further increasing rotation angle, the asymmetry shows a symmetrical change from 45° to 90°. The insets of Fig. 6(g) present the various magnetic images with various half-plate rotation angles. According to this relationship together with the comparable domain patterns obtained by circularly-polarized light, it is reasonable to conclude that the MLD contrast excited by DUV laser can be confirmed. This result suggests the same feasibility of linearly polarized laser on magnetic domain imaging as circularly polarized laser, which has been predicted by previous theoretical study [43].

4. Conclusion

In summary, magnetic contrast based on MCD/MLD was obtained in a PEEM excited by a DUV laser (λ = 177.3 nm and $h\upsilon$ = 7.0 eV) for the

first time. Due to the high photon energy, magnetic images can be clearly observed for oriented FePt films in MCD and MLD measurements without reducing the surface work function. Our results demonstrate that the DUV laser is a powerful source for magnetic domain imaging in combination with PEEM. The valence band structure and the density of states of FePt magnetic thin films should be further explored by using the DUV laser in order to have a deeper insight into the origin of the observed magnetic dichroic effects.

Acknowledgments

We thank Prof. Jia Li from Peking University for his helpful discussion and Prof. J. X. Zhang from Beijing Normal University for his help of MFM measurements. This work was supported by the Natural Science Foundation of China (Nos. 51625101, 51431009, and 51590880), the National Instrument Program of China (No. 2012YQ120048), the National Basic Research Program of China (No. 2015CB921401), and the Fundamental Research Funds for the Central Universities, China (No. FRF-TP-16-001C2).

References

[1] S.A. Wolf, D.D. Awschalom, R.A. Buhrman, J.M. Daughton, S. von Molnar, M.L. Roukes, A.Y. Chtchelkanova, D.M. Treger, Spintronics: a spin-based electronics vision for the future, Science 294 (2001) 1488–1495.
[2] D.A. Thompson, J.S. Best, The future of magnetic data storage technology, IBM J. Res. Dev. 44 (2000) 311–322.
[3] A. Hoffmann, S.D. Bader, Opportunities at the frontiers of spintronics, Phys. Rev. Appl. 4 (2015) 047001.
[4] H. Hopster, H.P. Oepen, Magnetic Microscopy of Nanostructures, first ed., Springer, Berlin; New York, 2004.
[5] E. Bauer, M. Mundschau, W. Swiech, W. Telieps, Surface Studies by Low-Energy Electron-Microscopy (LEEM) and Conventional UV Photoemission Electron-Microscopy (PEEM), Ultramicroscopy 31 (1989) 49–57.
[6] H.H. Rotermund, Imaging of dynamic processes on surfaces by light, Surf. Sci. Rep. 29 (1997) 267–364.
[7] J. Stöhr, Exploring the microscopic origin of magnetic anisotropies with x-ray magnetic circular dichroism (XMCD) spectroscopy, J. Magn. Magn. Mater. 200 (1999) 470–497.
[8] T. Funk, A. Deb, S.J. George, H.X. Wang, S.P. Cramer, x-ray magnetic circular dichroism - a high energy probe of magnetic properties, Coordin. Chem. Rev. 249 (2005) 3–30.
[9] B.P. Tonner, D. Dunham, T. Droubay, J. Kikuma, J. Denlinger, E. Rotenberg, A. Warwick, The development of electron spectromicroscopy, J. Electron. Spectrosc. 75 (1995) 309–332.
[10] H. Ohldag, T.J. Regan, J. Stöhr, A. Scholl, F. Nolting, J. Luning, C. Stamm, S. Anders, R.L. White, Spectroscopic identification and direct imaging of interfacial magnetic spins, Phys. Rev. Lett. 87 (2001) 247201.
[11] R. Moubah, M. Elzo, S. El Moussaoui, D. Colson, N. Jaouen, R. Belkhou, M. Viret, Direct imaging of both ferroelectric and antiferromagnetic domains in multiferroic $BiFeO_3$ single crystal using x-ray photoemission electron microscopy, Appl. Phys. Lett. 100 (2012) 042406.
[12] A.A. Sapozhnik, M. Filianina, S.Y. Bodnar, A. Lamirand, M.A. Mawass, Y. Skourski, H.J. Elmers, H. Zabel, M. Klaui, M. Jourdan, Direct imaging of antiferromagnetic domains in Mn_2Au manipulated by high magnetic fields, Phys. Rev. B 97 (2018) 134429.
[13] C.M. Schneider, G. Schönhense, Investigating surface magnetism by means of photoexcitation electron emission microscopy, Rep. Prog. Phys. 65 (2002) R1785–R1839.
[14] J. Wu, J. Choi, A. Scholl, A. Doran, E. Arenholz, Y.Z. Wu, C. Won, C.Y. Hwang, Z.Q. Qiu, Element-specific study of the anomalous magnetic interlayer coupling across NiO spacer layer in Co/NiO/Fe/Ag(001) using XMCD and XMLD, Phys. Rev. B 80 (2009) 012409.
[15] J. Li, A. Tan, K.W. Moon, A. Doran, M.A. Marcus, A.T. Young, E. Arenholz, S. Ma, R.F. Yang, C. Hwang, Z.Q. Qiu, Tailoring the topology of an artificial magnetic skyrmion, Nat. Commun. 5 (2014) 4704.
[16] W. Kuch, A. Dittschar, K. Meinel, M. Zharnikov, C.M. Schneider, J. Kirschner, J. Henk, R. Feder, Magnetic-circular-dichroism study of the valence states of perpendicularly magnetized Ni(001) films, Phys Rev B Condens Matter 53 (1996) 11621–11630.
[17] A. Rampe, G. Güntherodt, D. Hartmann, J. Henk, T. Scheunemann, R. Feder, Magnetic linear dichroism in valence-band photoemission: experimental and theoretical study of Fe(110), Phys. Rev. B 57 (1998) 14370–14380.
[18] W. Kuch, C.M. Schneider, Magnetic dichroism in valence band photoemission, Rep. Prog. Phys. 64 (2001) 147–204.
[19] G.K. Marx, H.J. Elmers, G. Schönhense, Magneto-optical linear dichroism in threshold photoemission electron microscopy of polycrystalline Fe films, Phys. Rev. Lett. 84 (2000) 5888–5891.
[20] T. Nakagawa, T. Yokoyama, Magnetic circular dichroism near the Fermi level, Phys. Rev. Lett. 96 (2006) 237402.
[21] T. Nakagawa, T. Yokoyama, M. Hosaka, M. Katoh, Measurements of threshold photoemission magnetic dichroism using ultraviolet lasers and a photoelastic modulator, Rev. Sci. Instrum. 78 (2007) 023907.
[22] T. Nakagawa, K. Watanabe, Y. Matsumoto, T. Yokoyama, Magnetic circular dichroism photoemission electron microscopy using laser and threshold photoemission, J. Phys. 21 (2009) 314010.
[23] M. Kronseder, J. Minar, J. Braun, S. Gunther, G. Woltersdorf, H. Ebert, C.H. Back, Threshold photoemission magnetic circular dichroism of perpendicularly magnetized Ni films on Cu(001): theory and experiment, Phys. Rev. B 83 (2011) 132404.
[24] K. Hild, J. Maul, T. Meng, M. Kallmayer, G. Schönhense, H.J. Elmers, R. Ramos, S.K. Arora, I.V. Shvets, Optical magnetic circular dichroism in threshold photoemission from a magnetite thin film, J. Phys. 20 (2008) 235218.
[25] T. Taniuchi, Y. Kotani, S. Shin, Ultrahigh-spatial-resolution chemical and magnetic imaging by laser-based photoemission electron microscopy, Rev. Sci. Instrum. 86 (2015) 023701.
[26] H.B. Michaelson, Work function of elements and its periodicity, J. Appl. Phys. 48 (1977) 4729–4733.
[27] L. Jin, Q. Fu, R. Mu, D. Tan, X. Bao, Pb intercalation underneath a graphene layer on Ru(0001) and its effect on graphene oxidation, Phys. Chem. Chem. Phys. 13 (2011) 16655–16660.
[28] X. Zhou, S. He, G. Liu, L. Zhao, L. Yu, W. Zhang, New developments in laser-based photoemission spectroscopy and its scientific applications: a key issues review, Rep. Prog. Phys. 81 (2018) 062101.
[29] C.T. Chen, J.H. Lu, T. Togashi, T. Suganuma, T. Sekikawa, S. Watanabe, Z.Y. Xu, J.Y. Wang, Second-harmonic generation from a $KBe_2BO_3F_2$ crystal in the deep ultraviolet, Opt. Lett. 27 (2002) 637–639.
[30] A. Locatelli, T.O. Mentes, M.A. Nino, E. Bauer, Image blur and energy broadening effects in XPEEM, Ultramicroscopy 111 (2011) 1447–1454.
[31] A. Kohn, N. Tal, A. Elkayam, A. Kovacs, D.L. Li, S.G. Wang, S. Ghannadzadeh, T. Hesjedal, R.C.C. Ward, Structure of epitaxial $L1_0$-FePt/MgO perpendicular magnetic tunnel junctions, Appl. Phys. Lett. 102 (2013) 062403.
[32] G. Yang, D.L. Li, S.G. Wang, Q.L. Ma, S.H. Liang, H.X. Wei, X.F. Han, T. Hesjedal, R.C.C. Ward, A. Kohn, A. Elkayam, N. Tal, X.G. Zhang, Effect of interfacial structures on spin dependent tunneling in epitaxial $L1_0$-FePt/MgO/FePt perpendicular magnetic tunnel junctions, J. Appl. Phys. 117 (2015) 083904.
[33] G.Q. Li, H. Takahoshi, H. Ito, H. Saito, S. Ishio, T. Shima, K. Takanashi, Morphology and domain pattern of $L1_0$ ordered FePt films, J. Appl. Phys. 94 (2003) 5672–5677.
[34] J. Stöhr, A. Scholl, T.J. Regan, S. Anders, J. Luning, M.R. Scheinfein, H.A. Padmore, R.L. White, Images of the antiferromaguetic structure of a NiO(100) surface by means of X-ray magnetic linear dichroism spectromicroscopy, Phys. Rev. Lett. 83 (1999) 1862–1865.
[35] T. Taniuchi, R. Yasuhara, H. Kumigashira, M. Kubota, H. Okazaki, T. Wakita, T. Yokoya, K. Ono, M. Oshima, M. Lippmaa, M. Kawasaki, H. Koinuma, Thickness dependence of magnetic domain formation in $La_{0.6}Sr_{0.4}MnO_3$ epitaxial thin films studied by XMCD-PEEM, Surf. Sci. 601 (2007) 4690–4693.
[36] O. Boulle, J. Vogel, H.X. Yang, S. Pizzini, D.D. Chaves, A. Locatelli, T.O. Mentes, A. Sala, L.D. Buda-Prejbeanu, O. Klein, M. Belmeguenai, Y. Roussigne, A. Stashkevich, S.M. Cherif, L. Aballe, M. Foerster, M. Chshiev, S. Auffret, I.M. Miron, G. Gaudin, Room-temperature chiral magnetic skyrmions in ultrathin magnetic nanostructures, Nat. Nanotechnol. 11 (2016) 449–454.
[37] M. Pickel, A.B. Schmidt, F. Giesen, J. Braun, J. Minar, H. Ebert, M. Donath, M. Weinelt, Spin-orbit hybridization points in the face-centered-cubic cobalt band structure, Phys. Rev. Lett. 101 (2008) 066402.
[38] P.C. McIntyre, C.J. Maggiore, M. Nastasi, Epitaxy of Pt thin films on (001)MgO .1. Interface energetics and misfit accommodation, Acta Mater. 45 (1997) 869–878.
[39] B.M. Lairson, M.R. Visokay, R. Sinclair, S. Hagstrom, B.M. Clemens, Epitaxial Pt (001), Pt(110), and Pt(111) Films on MgO(001), MgO(110), MgO(111), and Al_2O_3(0001), Appl. Phys. Lett. 61 (1992) 1390–1392.
[40] B.E. Nieuwenhuys, W.M. Sachtler, Crystal face specificity of nitrogen adsorption on a platinum field-emission tip, Surf. Sci. 34 (1973) 317–336.
[41] M.B. Holcomb, L.W. Martin, A. Scholl, Q. He, P. Yu, C.H. Yang, S.Y. Yang, P.A. Glans, M. Valvidares, M. Huijben, J.B. Kortright, J. Guo, Y.H. Chu, R. Ramesh, Probing the evolution of antiferromagnetism in multiferroics, Phys. Rev. B 81 (2010) 134406.
[42] A. Sander, M. Christl, C.T. Chiang, M. Alexe, W. Widdra, Domain imaging on multiferroic $BiFeO_3$(001) by linear and circular dichroism in threshold photoemission, J. Appl. Phys. 118 (2015) 224102.
[43] J. Henk, R. Feder, Magnetic circular dichroism in photoemission by linear polarized light, Phys. Rev. B 55 (1997) 11476–11482.